Assessment of Road Conditions on the University of Illinois Campus: Integrating Mobile, Drone, and Satellite Imagery

Hossein Kabir, Hamza Samouh, and Nishant Garg

Department of Civil and Environmental Engineering, University of Illinois at Urbana-Champaign, Urbana, IL, USA

Aug 2024

Abstract

Monitoring the condition of concrete and asphalt pavements is essential for ensuring their sustainability and structural integrity. Traditional road inspection methods are costly and dependent on the inspector's expertise. To overcome these limitations, we developed robust image-based techniques independent of operator skills. Our advanced algorithms for rapid image processing achieved a high correlation with traditional Pavement Condition Index (PCI) assessments (R^2 = 0.97). We integrated mobile, drone, and satellite imagery to assess road conditions on the University of Illinois campus, focusing on detecting and repairing distressed pavements. Data was collected from the B-1, E-14, and F-23 parking lots. Specifically, the F-23 lot showed significant degradation with ratios of 8.32% (iPhone), 7.91% (drone), and 7.64% (satellite). This project also focuses on repairing distressed concrete pavements on the University of Illinois campus, aiming to enhance their appearance. Thus, we propose practical methods for pavement repair, including preparation steps before applying our developed APTES-based penetrating sealant, which costs roughly 1/5th of a similar commercial product. This sealant with an application rate of 300 ft^2/ gal significantly enhances concrete durability by creating a hydrophobic layer, providing long-lasting protection against moisture and chemical intrusion.

Table of Contents

1. Introduction

The University of Illinois at Urbana-Champaign's pavement infrastructure, valued at over $49 million, is crucial for the smooth operation of campus activities, facilitating efficient movement and ensuring the safety of its community [1]. The management of this extensive 17.7 centerline mile network involves a robust pavement management system (PMS) that assesses the condition of 150 pavement sections, a system that has been periodically refined since its inception in 2009 to address evolving needs and conditions [1]. Traditionally, pavement condition assessments have been conducted using manual surveys based on ASTM D6433 standards [2], which are time-consuming and dependent on the skill and subjective judgment of the personnel involved. These surveys help calculate the Pavement Condition Index (PCI), critical for determining maintenance and rehabilitation priorities. Despite significant annual maintenance expenditures, the pavement condition has remained relatively stable over recent years, reflecting the challenges of maintaining an aging infrastructure with limited resources [1].

Recognizing the limitations of traditional methods, this report proposes a transformative approach by integrating mobile, drone, and satellite imagery to enhance the accuracy and efficiency of pavement condition assessments. Mobile imaging leverages the ubiquity of smartphones among students, allowing for extensive real-time data capture across campus [3]. This participatory approach not only facilitates immediate reporting of pavement distress but also enriches the dataset available for analysis, enabling more responsive maintenance strategies. Drone technology, equipped with advanced imaging capabilities, offers a comprehensive overview of road conditions from an aerial perspective [4]. This method provides detailed insights into areas that are challenging to assess at ground level, supporting a more thorough and accurate evaluation of pavement health. The integration of drone-captured data with ground observations creates a multi-dimensional resource for pavement management, enhancing the detection of deterioration and informing targeted interventions. Furthermore, satellite imagery serves as a strategic tool for macro-level monitoring and planning, offering consistent, large-scale views that are invaluable for long-term infrastructure management [5]. When combined with detailed data from drones and mobile devices, satellite images provide a full understanding of pavement conditions, supporting a practical approach to maintenance and rehabilitation. The synthesis of these imaging technologies into a unified assessment framework represents a significant advancement in pavement management, enabling the University to systematically address the diverse needs of its road network. By integrating mobile, drone, and satellite imagery, the PMS can rapidly assess the PCI of campus pavements, facilitating timely and effective maintenance decisions.

Addressing the practical aspects of pavement repair, especially the application of sealants, remains a pivotal challenge. Traditional commercial products are often costly and may not meet the specific needs of the campus environment. In response, our research team has developed a novel sealing material designed to be cost-effective and highly efficient for use in the University's diverse pavement conditions. This innovative product offers a sustainable alternative to conventional solutions, potentially reducing the financial burden of pavement maintenance while extending the lifespan and enhancing the functionality of the road network. In summary, this report advocates for a strategic overhaul of pavement management practices at the University of Illinois, harnessing cutting-edge technologies and innovative materials to transform how pavement conditions are monitored and maintained. Through the integration of mobile, drone, and satellite imagery,

coupled with the development of a new penetrating sealant, the University aims to achieve a more resilient and sustainable pavement infrastructure, reflecting a commitment to safety, efficiency, and fiscal responsibility.

2. Traditional Approach for Measuring PCI

The PCI of concrete and asphalt pavements is traditionally measured through a detailed visual inspection process conducted by trained personnel who survey the pavement surface methodically [2]. This involves identifying, recording, and classifying various types of pavement distresses such as cracks, potholes, rutting, raveling, and surface deformations. Inspectors use a predefined sample unit, typically a section of the pavement, and assess the type, severity, and extent of each distress. Severity levels are categorized as low, medium, or high, and the extent is measured as the percentage of the area affected. This process requires inspectors to follow standardized guidelines and protocols to ensure consistency and accuracy in the data collection. The collected data is then analyzed using established algorithms that convert the distress information into a numerical PCI score ranging from 0 to 100, where 0 represents a failed pavement and 100 indicates an excellent condition. The PCI score helps in determining the current state of the pavement and identifying maintenance and rehabilitation needs. This traditional manual method, while providing a comprehensive and detailed assessment, is labor-intensive, time-consuming, and subject to human error.

3. Automated Pavement Condition Assessment via Distressed Ratio Analysis

In recent years, advancements in image processing and computer vision have enabled more efficient and objective methods for assessing pavement conditions [3-5]. An alternative approach involves analyzing pavement distress using image binarization techniques to calculate the distressed area ratio, which can be correlated with the PCI. Our robust method leverages algorithms to identify and quantify the extent of visible cracks and other surface deformations on pavement images. By converting the image to a binary format where the distressed areas are highlighted, the percentage of white pixels in the binary image represents the distressed ratio. This ratio can be systematically compared to traditional PCI scores to develop a robust correlation, streamlining the assessment process.

Using the provided code (**Figure 1**), pavement crack images are processed to calculate the white pixel ratio. The code reads the pavement image using OpenCV, converts it to grayscale, and optionally applies Gaussian blur to reduce noise. It then binarizes the image with a thresholding technique (`cv2.threshold`), turning pixels above a certain intensity white (255) and those below black (0), effectively highlighting cracks. The number of white pixels is calculated (`np.sum(thresh == 255)`), and divided by the total number of pixels to compute the distressed ratio, expressed as a percentage. The original and binary images are displayed for visual comparison, showing the white pixel ratio (WPR). Thus, by establishing a reliable correlation between the distressed area ratio and PCI, this approach would offer a promising alternative to traditional manual inspections, ensuring consistency and minimizing human error. The developed Python code, shown in **Figure 1**, details the entire process of calculating the distressed area ratio from pavement images.

```
import cv2
import numpy as np
from matplotlib import pyplot as plt

# Reading the image
img = cv2.imread('/kaggle/input/crack-vs-pci/1.JPG', 0)

# Image binarization
_, thresh = cv2.threshold(img, 144, 255, cv2.THRESH_BINARY_INV)

# Calculate the ratio of white to all pixels
white_ratio = np.round(np.sum(thresh == 255) / thresh.size * 100, 2)

# Plotting
plt.figure(figsize=(10, 10))
plt.subplot(121), plt.imshow(img, cmap='gray')
plt.title('image id = 1', fontsize=20), plt.xticks([]), plt.yticks([])
plt.subplot(122), plt.imshow(thresh, cmap='gray')
plt.title(f'white pixel ratio = {white_ratio}%', fontsize=20), plt.xticks([]), plt.yticks([])

print(white_ratio)

plt.savefig('analyzed_1.png', dpi=150, bbox_inches='tight')
```

Figure 1: Analysis of distress detection in a pavement image using our threshold-based binarization method.

3.2. Crack Detection in Parking Lots: Drone vs. Mobile and Satellite Imagery

To showcase the effectiveness of our algorithm in detecting distresses and cracks, we flew our drone over several parking lots at different elevations and calculated the corresponding distress area ratios (white pixel ratios, WPRs). We then compared these results with those obtained from mobile and satellite images. The comparison confirmed the accuracy and reliability of our approach in various imaging conditions. The drone images were captured using the DJI Mini 2 at the University of Illinois B-1 parking lot, see **Figure 2**. This lot is usually crowded near the library entrances, so the northeast section was chosen for its relative safety. The pavement in this area is asphalt and generally in poor condition. The images focused on cracks with minimal debris. Although there are many cracks throughout the lot, areas with constant traffic were avoided. Photos were taken in the early afternoon (1 pm to 3 pm) under partly sunny conditions. Each crack was photographed at heights of 1ft, 5ft, 10ft, 15ft, 20ft, 25ft, and 30ft. Additionally, images were taken using an Apple iPhone 13 mini at a height of 3 feet and Google Earth Pro Satellite Imagery. The results of our crack detection algorithm applied to images captured at various elevations reveal distinct patterns in the WPR, indicating the crack area. At lower elevations (1 ft to 15 ft), the WPR shows more variation, with the highest at 1 ft (8.65%) and 15 ft (7.74%). This is due to the higher resolution and proximity to the cracks, allowing finer details to be captured. As the elevation increases, the WPR stabilizes, particularly between 20 ft and 30 ft, suggesting a balance between image resolution and area coverage. Interestingly, the satellite imagery, despite being captured at a significantly higher elevation, shows a WPR of 6.44%, which aligns with the ratios obtained at 20 ft and 30 ft. This consistency underscores the robustness of the algorithm in maintaining accuracy across different scales.

The graph plotting WPR against ground elevations further supports these observations, showing a general trend of stability in the middle elevation range. Overall, the analysis indicates that while lower elevations capture more detail, higher elevations provide sufficient accuracy for practical purposes. The satellite imagery's comparable performance highlights the potential for large-scale monitoring without compromising on detection reliability. The study reinforces the effectiveness of drone imagery in bridging the gap between high-detail mobile images and extensive satellite views, offering a versatile solution for infrastructure monitoring. The importance of analyzing the WPR lies in its direct correlation with the visibility and detectability of cracks. By examining the images at various elevations, we can determine the optimal height for capturing clear and actionable data. The higher WPR at lower elevations is expected due to the enhanced detail captured by the drone's camera. However, as the elevation increases, the decrease in resolution is offset by the broader field of view, which helps maintain a relatively stable WPR. Moreover, the consistent performance of the algorithm at higher elevations and in satellite imagery suggests its robustness and adaptability to different image qualities and scales. This versatility is crucial for practical applications, where consistent and reliable detection of cracks and distresses is necessary for maintenance and monitoring.

The drone images were also captured at the University of Illinois E-14 and F-23 parking lots, shown in **Figure 3**. For the E-14 lot, the images were taken in the southern area, which was relatively safer due to the high occupancy near the entrances. The pavement in this section is asphalt, with significant color differences indicating varied materials or ages. Images were taken in the early morning to midday (8 am to 1 pm) under partly sunny to partly cloudy conditions. All cracks were photographed near each other to ensure consistency in the material and pavement age, including two horizontal cracks and one vertical crack. For the F-23 lot, images were also taken in the southern area for safety reasons due to high occupancy near the entrances. The pavement consists of very old asphalt and gravel. Many cracks appeared to have been repaired or filled with plants or debris, but the images focused on cracks without these conditions. The cracks included various vertical and horizontal cracks. Photos were taken in the early afternoon (12 pm to 2 pm) under partly sunny conditions. Again, for both parking lots, Each surface distress was photographed at heights of 15ft. Moreover, images were taken using an Apple iPhone 13 mini at a height of 3 feet and Google Earth Pro Satellite Imagery. The ratio of white pixels, which represent the cracks, is extremely low across all elevations—1.05% at 3 feet using a phone, 0.04% at 15 feet using a drone, and 0.05% in satellite imagery. This indicates that the E-14 lot has very few surface distresses. In contrast, the F-23 lot shows significant cracking, with the ratio of white pixels being considerably higher—8.32% at 3 feet using a phone, 7.91% at 15 feet using a drone, and 7.64% in satellite imagery. This highlights the severe degradation and cracking present in the F-23 lot. The higher WPRs indicate a larger area affected by cracks, emphasizing the poor condition of the F-23 lot compared to the well-maintained E-14 lot.

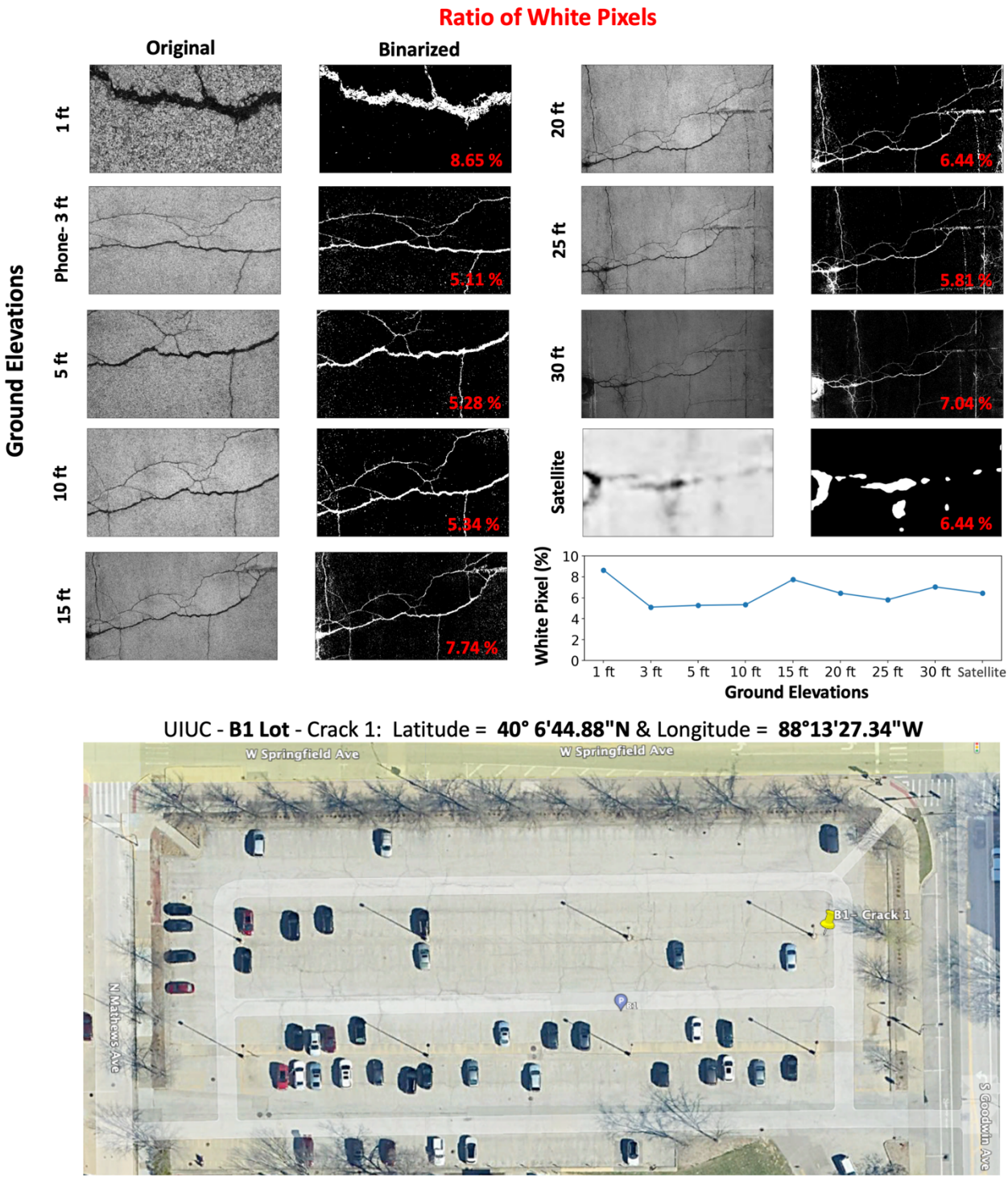

Figure 2: Comparative Analysis of Crack Detection at Various Elevations in UIUC B-1 Lot. This figure illustrates the crack detection results from different imaging sources and heights in the UIUC B-1 parking lot: drone images at elevations from 1 ft to 30 ft, a mobile image at 3 ft, and satellite imagery. Each set of images includes the original and binarized versions with the WPR indicating the crack area. The graph plots the WPR against the corresponding elevations. The bottom image shows the specific location in the B-1 parking lot where the study was conducted.

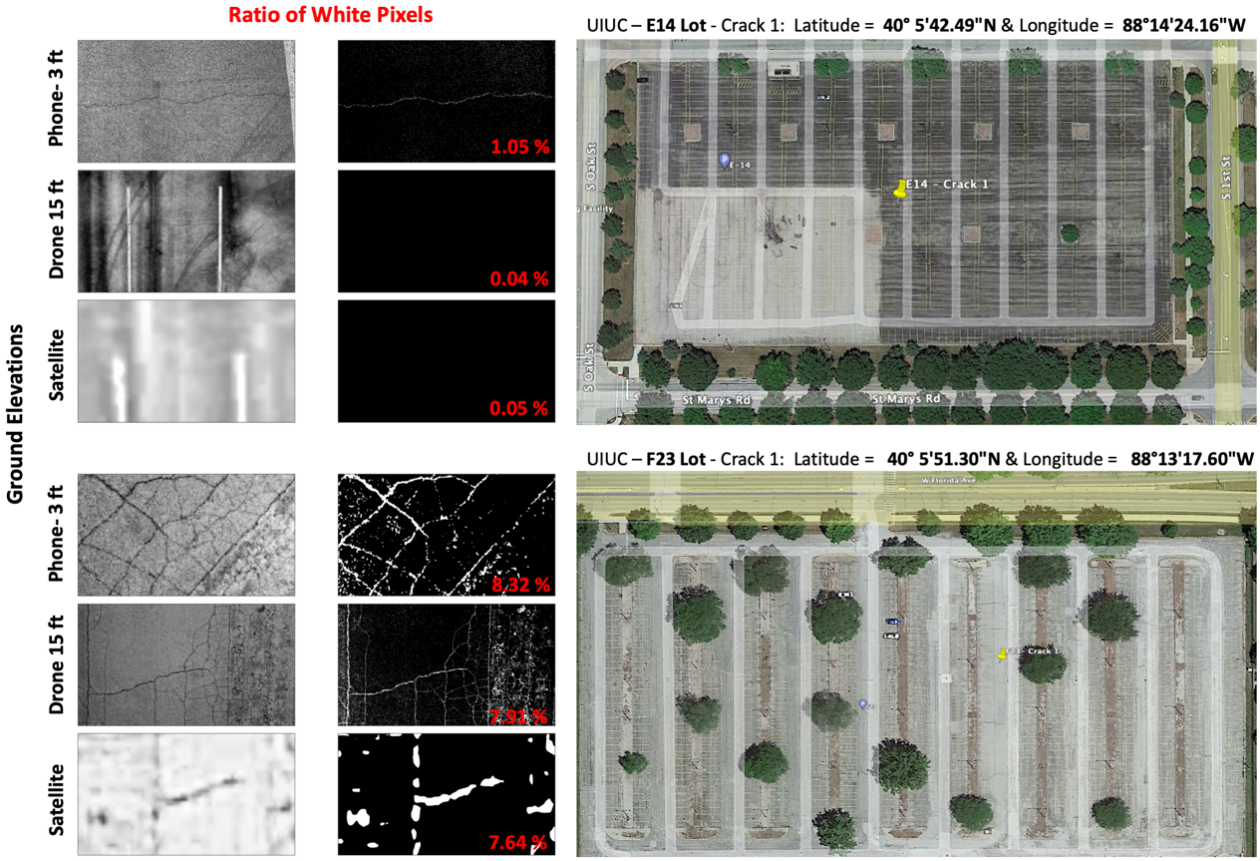

Figure 3: Analysis of pavement cracks at UIUC's E-14 and F-23 parking lots. Images from an iPhone (3 ft), a drone (15 ft), and a satellite show minimal cracking in E-14 (WPRs: 1.05%, 0.04%, 0.05%) and significant cracking in F-23 (8.32%, 7.91%, 7.64%). The E-14 lot is in very good condition, while the F-23 lot shows severe degradation. Maps indicate crack locations.

3.3. Correlation Analysis Between Distress Area Ratios and PCI

Following the fine-tuning of our algorithms in the previous steps, we are now interested in determining whether any correlations could be established between the distress area ratios and the Pavement Condition Index (PCI). For this purpose, we selected 42 random images from the appendix of U20069: Pavement Analysis Study 2020, University of Illinois at Urbana-Champaign, and extracted their WPRs. It should be noted that photos 1-21 are shown in **Figure 4**, while photos 22-42 are shown in **Figure 5**. These images were selected to cover a relatively broad range of surface distress that appeared on various pavement types, including AAC (asphalt overlay of asphalt pavement), AC (asphalt concrete pavement), APC (asphalt overlay of PCC pavement), and PCC (concrete pavement).

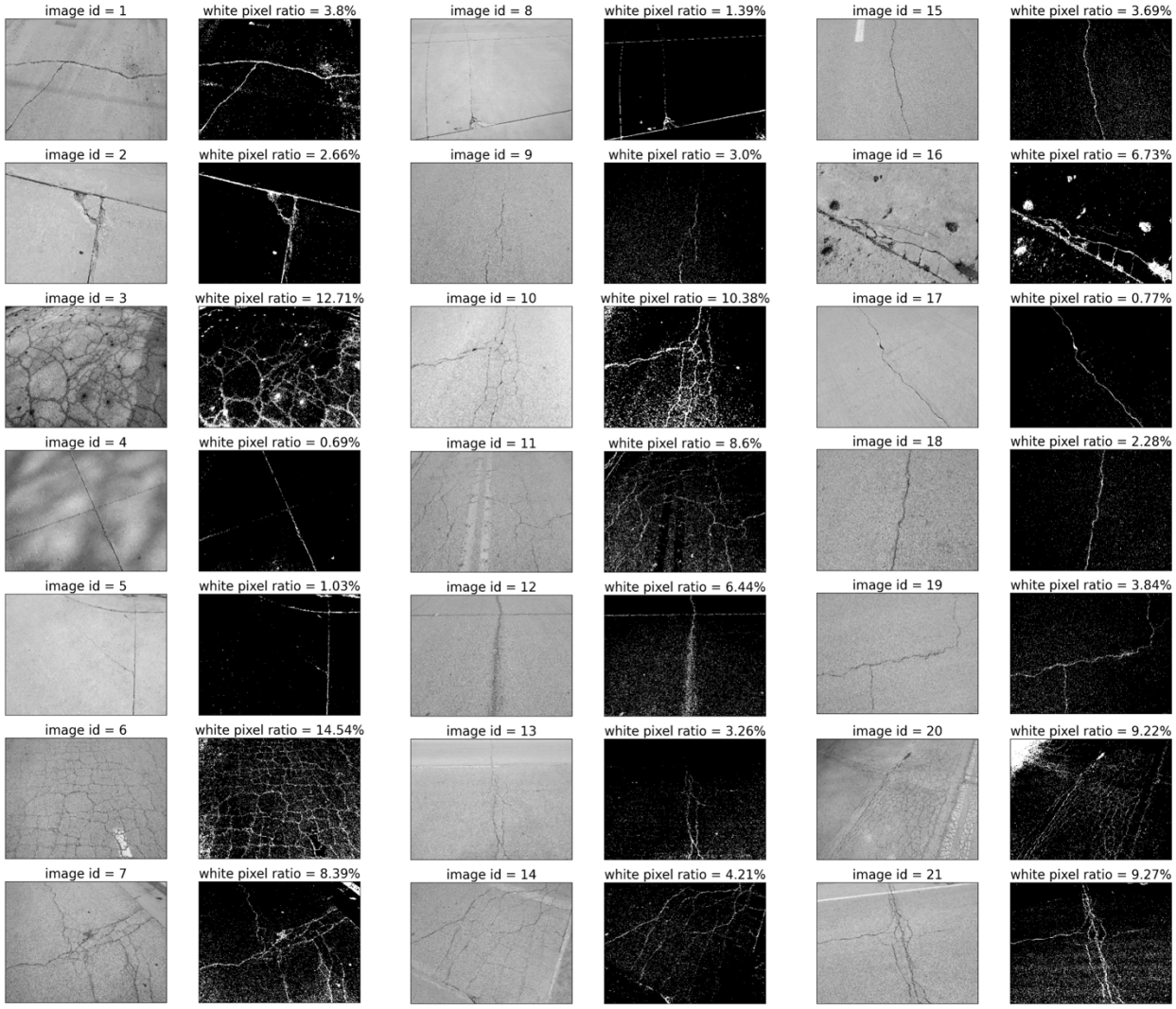

Figure 4: Selected 21 images from U20069: Pavement Analysis Study 2020, University of Illinois at Urbana-Champaign. Extracted WPRs to explore correlations with the Pavement Condition Index (PCI). Images cover various surface distresses in AAC, AC, APC, and PCC pavements.

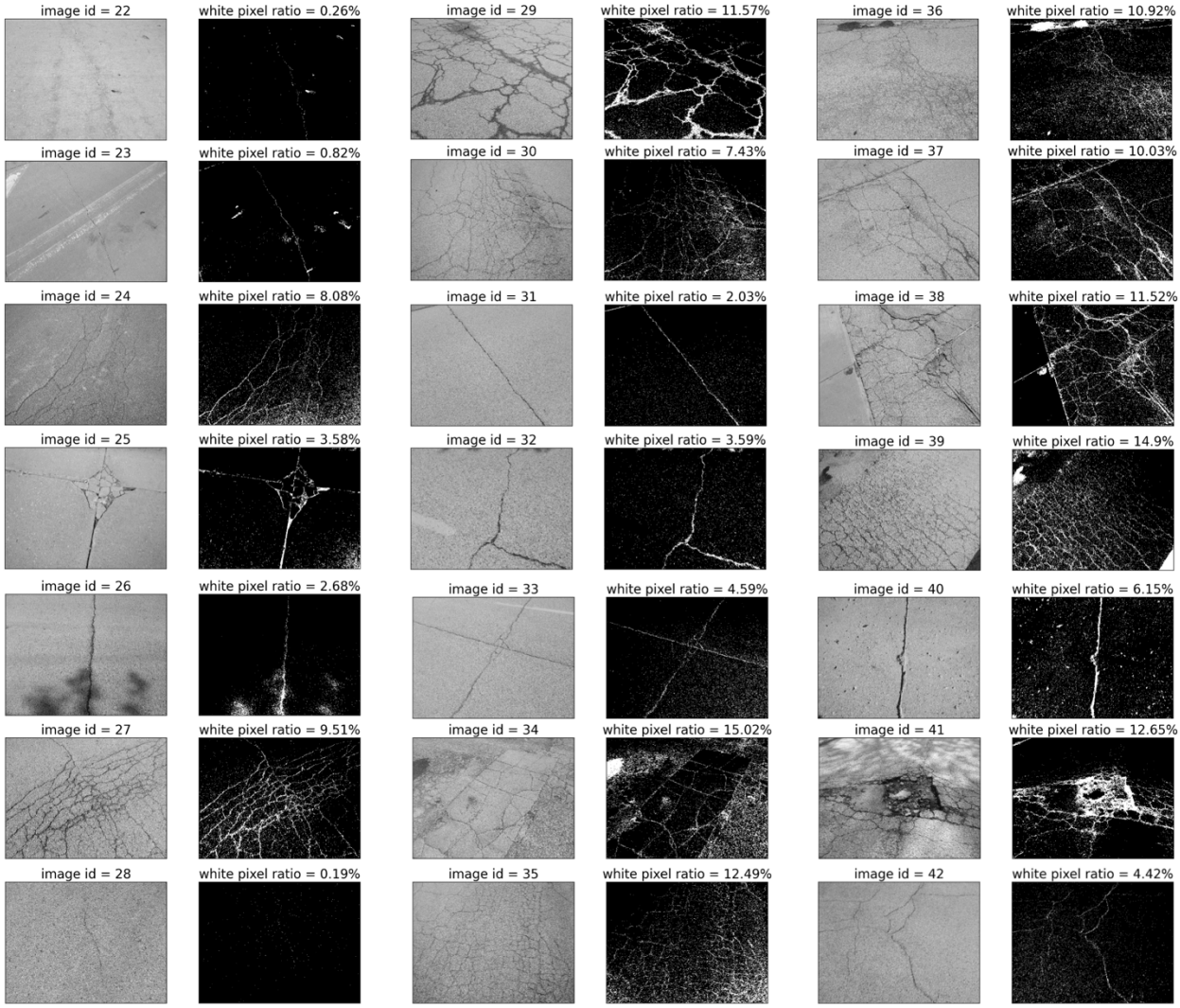

Figure 5: Selected 21 additional images from U20069: Pavement Analysis Study 2020, University of Illinois at Urbana-Champaign. Extracted WPRs to investigate correlations with the Pavement Condition Index (PCI). Images represent a range of surface distresses in AAC, AC, APC, and PCC pavements.

Figure 6a provides a detailed summary of the selected images, listing the branch id, section id, surface type, PCI, and the WPR (representing the distress area ratio) for all 42 images explained in **Figures 4** and **5**. This comprehensive table is critical for understanding the relationship between surface distress and PCI across different pavement types. **Figure 6b** displays the distributions of PCI for different surface types (AC, APC, PCC, and AAC). The first subplot illustrates the frequency distribution of PCI values for AC surfaces, showing a relatively uniform distribution across various PCI ranges. The second subplot, focusing on APC surfaces, shows a concentration of PCI values around the mid-range. The third subplot, for PCC surfaces, indicates a higher frequency of PCI values towards the upper range. The final subplot for AAC surfaces shows a narrower distribution with most PCI values concentrated at the higher end. These histograms provide insights into the condition distribution of different pavement types. **Figure 6c** highlights the strong correlation between the distress area ratio (WPR) and PCI. The scatter plot clearly shows a negative correlation, indicating that as the distress area increases, the PCI decreases. The

established formula, PCI (2020) = - 6.11 × WPR + 94.61, quantifies this relationship. This linear regression model, with an R^2 value of 0.97, demonstrates a high level of accuracy in predicting PCI based on the distress area ratio. This finding is crucial for pavement maintenance and management, allowing for more accurate assessments of pavement conditions based on visual distress metrics.

a

image id	branch id	section id	surface	pci	white pixel ratio	image id	branch id	section id	surface	pci	white pixel ratio
1	ARMRYA	E00	PCC	69	3.8	22	GREGYD	E03B	PCC	94	0.26
2	ARMRYA	E05	PCC	78	2.66	23	GREGYD	E04	PCC	84	0.82
3	BAILEYD	E00	AC	18	12.71	24	GREGYD	UW10	AC	48	8.08
4	CLARKST	UW12	PCC	90	0.69	25	GREGYD	UW12D	PCC	68	3.58
5	CLARKST	UW12	PCC	90	1.03	26	HAZELWDD	E00A	AC	62	4.32
6	COLAGCT	UW09AS	AC	3	14.54	27	HAZELWDD	E00C	AC	35	9.51
7	COLAGCT	UW09BN	AC	44	8.39	28	HAZELWDD	UW04	AC	94	0.19
8	COLAGCT	UW09CN	PCC	85	1.39	29	KIRKD	S20B	AC	25	11.57
9	DORNRDR	US11AE	APC	76	3	30	LORADOTD	UW12	AC	47	7.43
10	DORNRDR	US11AW	APC	30	10.38	31	OAKS	S18B	AAC	81	2.03
11	DORNRDR	US13E	AC	41	8.6	32	OAKS	S20A	AC	73	3.59
12	VRGNADR	US14A	APC	53	6.44	33	PEABYD	E03	APC	65	4.59
13	FIRSTS	S15	APC	75	3.26	34	PEABYD	E06A	AC	3	15.02
14	FOURTS	S11	AAC	70	4.21	35	PENSYA	UW12B	AC	16	12.49
15	FOURTS	S12	APC	71	3.69	36	SIXTHS	S11	APC	32	10.92
16	GERTYD	E00B	PCC	54	6.73	37	SIXTHS	S13	APC	34	10.03
17	GERTYD	E00D	PCC	88	0.77	38	STADMD	E00A	AC	25	11.52
18	GHUFFDR	UW04AN	AAC	81	2.28	39	STMARR	E00A	AC	5	14.9
19	GHUFFDR	UW04BN	AAC	64	3.84	40	STMARR	E00B	PCC	52	6.15
20	GOODWINA	US08	APC	36	9.22	41	STMARR	E00D	APC	19	12.65
21	GREGYD	E01AS	APC	32	9.27	42	STMARR	E04B	AC	68	4.42

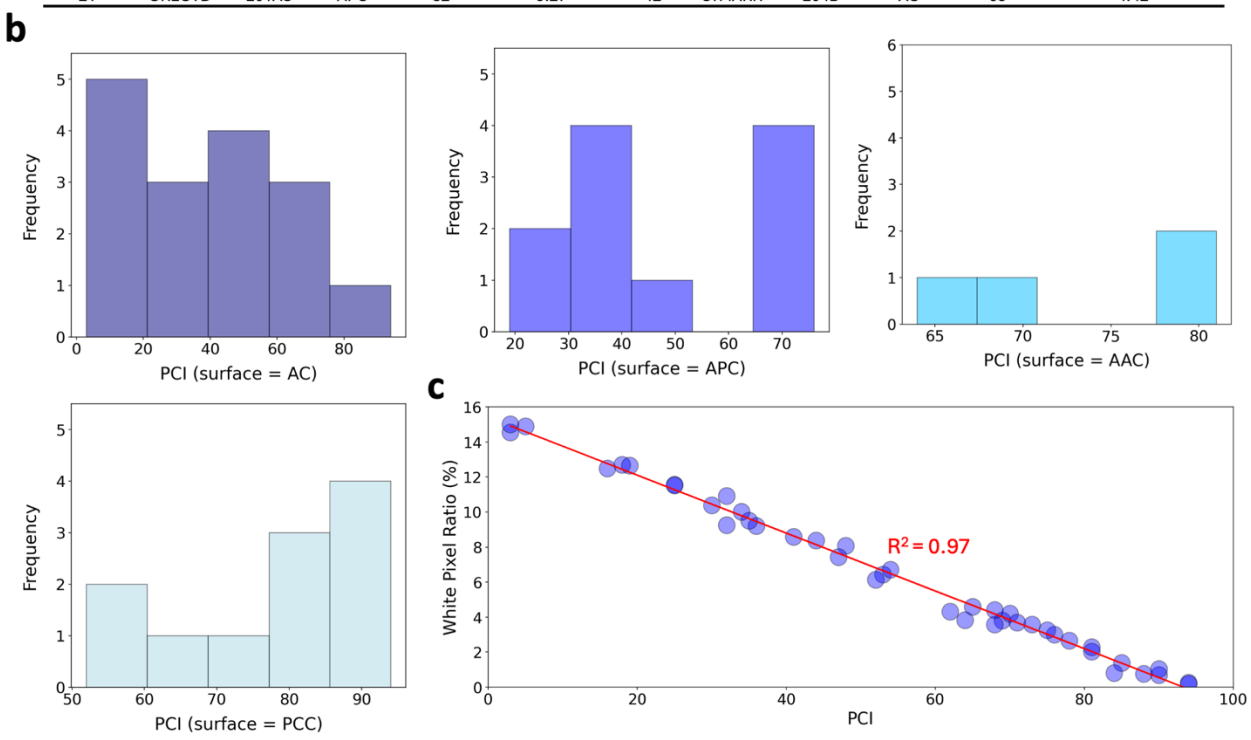

Figure 6: (a) Summary of 42 images, listing branch id, section id, surface type, Pavement Condition Index (PCI), and WPR (distress area ratio). Photos 1-21 are from Figure 4; photos 22-42 are from Figure 5. (b) Frequency distributions of PCI values for AC, APC, PCC, and AAC surfaces. (c) Scatter plot showing the strong negative correlation between distress area ratio and PCI, with an R^2 value of 0.97. The regression line represents Estimated PCI (2020) = -6.11 × WPR + 94.61.

Figure 7 illustrates the comparison between the traditional method and the proposed satellite imagery method for assessing pavement conditions. The proposed method leverages satellite imagery data to calculate the distress area ratio and subsequently estimate the PCI for campus pavements. This approach offers an inexpensive and rapid analysis of pavement conditions at any time, providing higher resolution compared to the subjective, expensive, and manual traditional method.

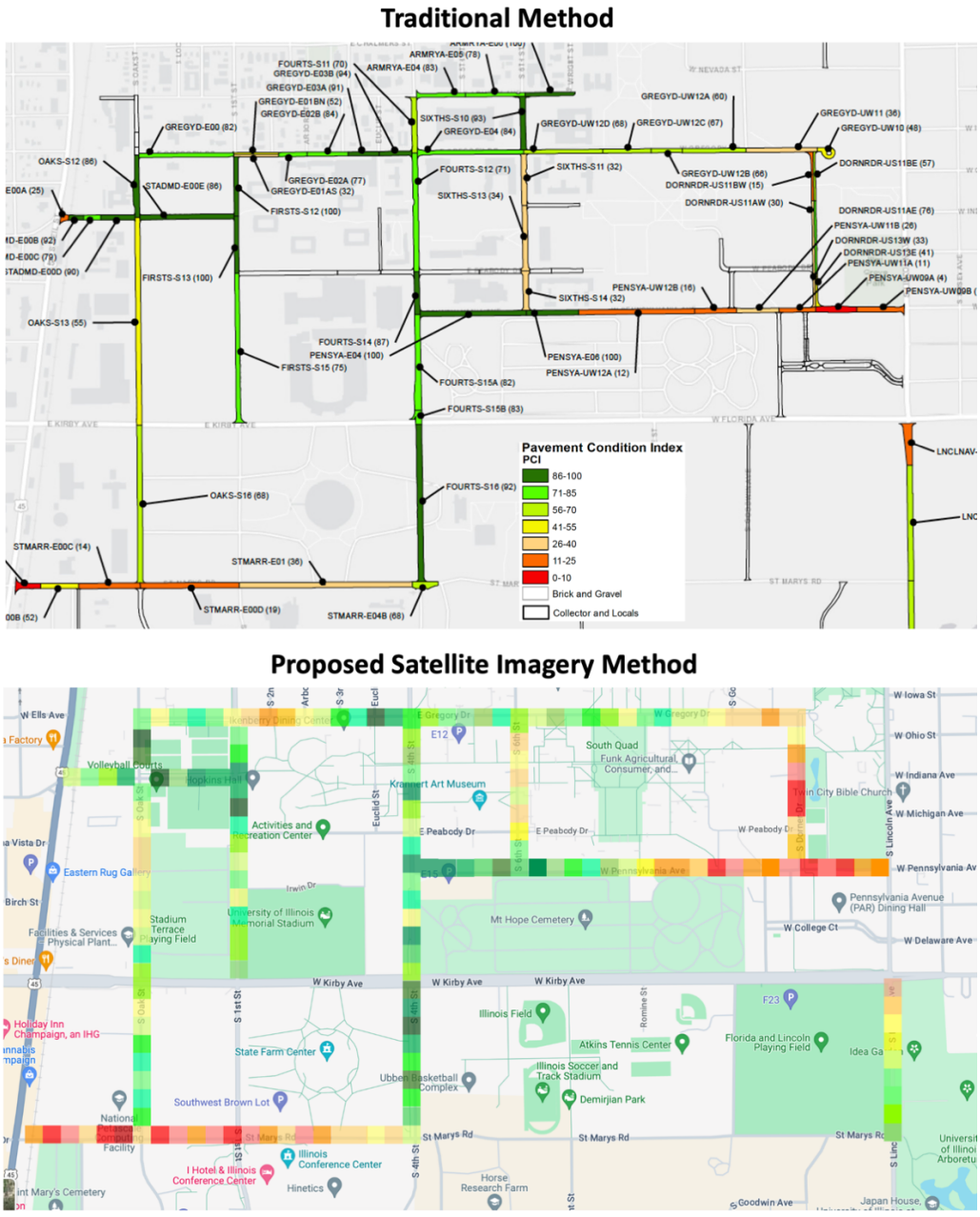

Figure 7: Comparison of pavement condition assessment methods using satellite imagery for a detailed, cost-effective, and timely analysis versus the traditional manual approach.

4. Repair Methods for Concrete Pavements

In this section, we explore the various methods employed for repairing concrete pavements. By examining these methodologies, we aim to provide a comprehensive understanding of the best practices for maintaining and extending the lifespan of concrete infrastructures.

4.1. Repairing Concrete Overlays/Pavements

When extensive cracking occurs on concrete overlays/pavements, a patch is cut and replaced with a fresh concrete overlay, exposing and addressing corroded steel reinforcement and marked reflecting cracks. The substrate is moistened, filled with fresh concrete, smoothed with a steel trowel, and cured for at least three days before reopening to traffic, though this method is slow and costly, making it suitable only for significantly distressed areas. An alternative method involves repairing cracks, which requires widening the cracks (**Figure 8a**), cleaning with compressed air (**Figure 8b**), and manually applying the two-part epoxy (**Figure 8c**). Despite being labor-intensive and costly, epoxy offers a durable solution but lacks flexibility and stability on sloped surfaces, and is best applied in warmer temperatures. Another method involves using CRAFCO rubber, which is melted and applied to cracks, offering a faster, cheaper solution suitable for wider cracks and colder conditions, though it requires annual reapplication due to its shorter lifespan compared to epoxy, see **Figure 8d**.

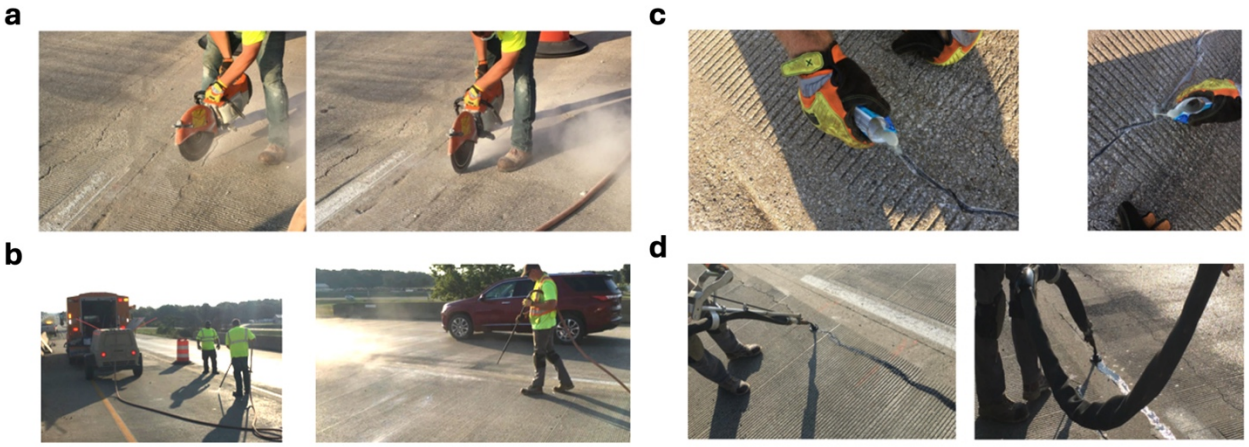

Figure 8: Repair methods for extensive cracking on concrete overlays/pavements. (a) Cracks are widened using saw-cut equipment. (b) Compressed air is used to clean debris from the cracks. (c) Two-part epoxy sealant is manually applied to the cleaned cracks. (d) CRAFCO rubber is melted and applied to the cracks, providing a faster and cheaper solution suitable for wider cracks and colder conditions, although it requires annual reapplication due to its shorter lifespan compared to epoxy.

4.2. Penetrating Sealants for Concrete Overlays/Pavements

Penetrating sealers, such as silanes, siloxanes, silicates, and siliconates, are essential for protecting concrete from moisture intrusion and aggressive deicing chemicals. These sealers form a chemical barrier within the concrete, providing invisible protection without altering the surface appearance and allowing moisture vapor to escape. This breathable characteristic makes them ideal for outdoor applications where concrete is exposed to harsh conditions. Among various silanes available, (3-Aminopropyl) triethoxysilane (APTES) stands out due to its ability to bond with hydrated cement paste and create a hydrophobic layer, making it an excellent candidate for a penetrating sealant, see **Figure 9** [6].

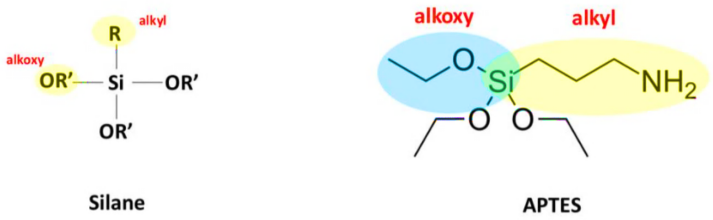

Figure 9: General chemical structure of silanes (left), the chemical structure of APTES (right).

To develop the penetrating sealant, APTES was chosen for its unique chemical properties. APTES was purchased from Gelest, Inc., selected for its cost-effectiveness and availability. The sealant was prepared by mixing APTES with ethanol, graphene oxide, and stearic acid, followed by hydrolysis using a vortex mixer, see **Table 1** for the mix design. This process converted the hydrolyzable groups into hydroxyl groups, enabling the silane to penetrate the concrete more effectively and bond with its surface.

Table 1: Mix design for our developed APTES-based penetrating sealant.

Material Name	Volume or Weight	pH
Stearic Acid	0.07 g	6
APTES	56 µl	7
Ethanol	7.5 ml	7.3
Graphene Oxide	0.001 g	10.5

The sealant was then applied to cement paste specimens to evaluate its effectiveness in enhancing hydrophobicity. The treated specimens shown in **Figure 10a**, proved a significant increase in contact angles, demonstrating the sealant's ability to create a water-repellent surface. To go further, **Figure 10b** schematically represents the reaction mechanism of silica functionalization by APTES in the presence of water [7]. In this reaction, the hydrolyzable groups of $(OCH_2CH_3)^-$ in the structure of APTES are converted into OH^- (hydroxyl) groups in a process called hydrolysis. After the formation of hydroxyl groups in the hydrolyzed APTES, the solution can be sprayed onto concrete to create a strong Si-O-Si bond through condensation, as shown in **Figure 10c** [8]. During this process, water gradually evaporates, rendering the surface hydrophobic. As illustrated in **Figure 10d**, it is evident that the developed sealant can reduce mass change and increase the hydrophobicity of the specimen. It should be noted that the authors have previously demonstrated a strong correlation between surface wettability and absorption of cement pastes, which is also

evident in this figure [9]. Additionally, surface wettability can be measured using an inexpensive goniometer, making this approach both practical and cost-effective [10]. Thus, our developed sealant effectively protects the concrete surface from the intrusion of aggressive solutions such as chloride ions.

It should be noted that when the solid surface is hydrophilic (contact angle < 90°), the apparent contact angle decreases as the surface roughness increases. Conversely, if the solid surface is hydrophobic (contact angle > 90°), the apparent contact angle increases with the surface roughness [11]. Consequently, the cement pastes were sandblasted for 2 seconds and treated with our APTES-based sealant, resulting in an average contact angle increase of 10-20% (**Figure 10e**). As shown in this figure, the samples were cut in half, and the cross-sections were sprayed with water, demonstrating that the percentage of the area that changed color (from bright to dark) is smaller for the sandblasted specimen, proving the benefits of surface sandblasting on the penetration of our sealants. Also, as shown in **Table 2**, our developed penetrating sealant (with an application rate of 300 ft^2/ gal.) has a cost of roughly 1/5th of the similar commercial product. Thus, this APTES-based sealant proved to be a cost-effective and efficient solution for improving the durability of concrete structures, offering long-lasting protection against moisture and chemical intrusion.

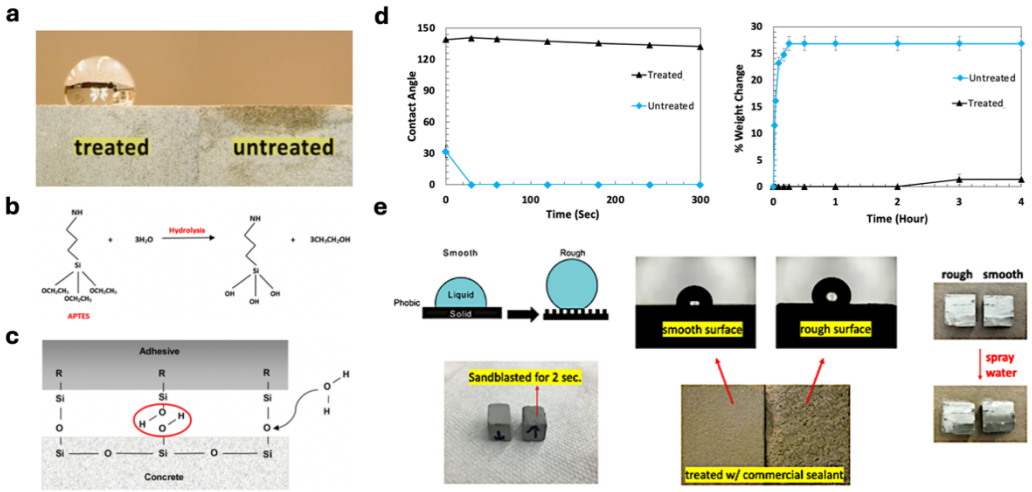

Figure 10: Evaluation of the sealant's effectiveness on cement paste specimens. (a) Contact angle comparison between treated and untreated specimens, showing enhanced hydrophobicity. (b) Reaction mechanism of silica functionalization by APTES in water. (c) Formation of strong Si-O-Si bonds on concrete surfaces, creating hydrophobicity. (d) Graphs showing reduced mass change and increased hydrophobicity, protecting concrete from chloride ions. (e) Effect of surface roughness; sandblasting and APTES treatment increased contact angle by 10-20%. Cross-sections sprayed with water show smaller color changes in sandblasted specimens, indicating deeper sealant penetration.

Table 2: Cost per gallon of our produced penetrating APTES-based silane.

Material	**Cost $ / gal**
Stearic Acid	1
APTES	20
Ethanol	15
Graphene Oxide	2
Total	**38**
Commercial Penetrating Sealers	**150-200**

5. Conclusions

In this study, we integrated mobile, drone, and satellite imagery for assessing pavement conditions on the University of Illinois campus, which demonstrated significant advancements in both accuracy and efficiency. Our image-based techniques achieved a high correlation ($R^2 = 0.97$) with traditional Pavement Condition Index (PCI) assessments, confirming the reliability of our methods. Specifically, our analysis revealed that the F-23 parking lot exhibited the most severe degradation with distress ratios of 8.32% (iPhone), 7.91% (drone), and 7.64% (satellite), highlighting the effectiveness of our approach in diverse imaging conditions. Moreover, our research extended to developing a novel APTES-based penetrating sealant, which costs roughly 1/5th of similar commercial products and significantly increased the hydrophobicity and durability of concrete pavements, demonstrated by an application rate of 300 ft^2/gal. This sealant effectively creates a hydrophobic layer, enhancing protection against moisture and chemical intrusion. This comprehensive approach not only enhances the accuracy and efficiency of pavement condition monitoring but also provides cost-effective and durable solutions for pavement repair, ensuring sustainable and resilient infrastructure management on campus.

6. Future Directions

Our current work has primarily focused on drone imagery of parking lots, and in the future, we aim to extend this to all campus roads. This expansion will significantly enhance the PCI resolution compared to satellite imagery, providing a more comprehensive and detailed assessment of pavement conditions. Additionally, while our proposed APTES-based penetrating sealant has shown promising results when applied to lab samples, future plans include applying this sealant to larger pavement sections in the field. This will allow us to evaluate its performance on a more realistic scale and assess its long-term effectiveness in protecting and maintaining campus pavements. Furthermore, we plan to explore the environmental impact of our APTES-based penetrating sealant to ensure that it is a sustainable and eco-friendly solution. By implementing these advancements, we aim to improve the accuracy of our pavement condition assessments and the durability of our repair solutions, contributing to a more sustainable infrastructure management system on campus.

7. Acknowledgements

The authors would like to express their sincere gratitude for the support received from Stacey DeLorenzo and Sarthak Prasad, whose invaluable guidance and assistance were instrumental in the successful execution of this project. We also extend our appreciation to Andrea Nava, an undergraduate student, who assisted in capturing phone and drone images during this study. Additionally, we are grateful to the UIUC Facilities and Services for providing the necessary resources and logistical support, which were crucial for the extensive fieldwork and data collection efforts. Finally, we thank the UIUC Department of Civil and Environmental Engineering and the Student Sustainability Committee (SSC) for their generous funding and support. This work would not have been possible without the collaborative efforts and contributions of these individuals and organizations.

8. References

[1] U20069: Pavement Analysis Study, University of Illinois at Urbana-Champaign, **2020**.

[2] ASTM D6433-16 Standard Practice for Roads and Parking Lots Pavement Condition Index Surveys. West Conshohocken, PA, USA, **2017**.

[3] Farhadmanesh, M., Cross, C., Mashhadi, A. H., Rashidi, A., & Wempen, J. Highway asset and pavement condition management using mobile photogrammetry. *Transportation Research Record*, 2675(9), 296-307, **2021**.

[4] Pietersen, R. A., Beauregard, M. S., & Einstein, H. H. Automated method for airfield pavement condition index evaluations. *Automation in Construction*, 141, 104408, **2022**.

[5] Bashar, M. Z., & Torres-Machi, C. Exploring the capabilities of optical satellite imagery in evaluating pavement condition. *In Construction Research Congress*, pp. 108-115, **2022**.

[6] Elvers, B. Ullmann's encyclopedia of industrial chemistry (p. 9). *Verlag Chemie*, **1991**.

[7] Brochier Salon, M. C., & Belgacem, M. N. Hydrolysis-condensation kinetics of different silane coupling agents. *Phosphorus, Sulfur, and Silicon*, 186(2), 240-254, **2011**.

[8] Chiong, S. J., Goh, P. S., & Ismail, A. F. Novel hydrophobic PVDF/APTES-GO nanocomposite for natural gas pipelines coating. *Journal of Natural Gas Science and Engineering*, 42, 190-202, **2017**.

[9] Kabir, H., & Garg, N. Rapid prediction of cementitious initial sorptivity via surface wettability. *npj Materials Degradation*, 7(1), 52, **2023**.

[10] Kabir, H., & Garg, N. Machine learning enabled orthogonal camera goniometry for accurate and robust contact angle measurements. *Scientific Reports*, 13(1), 1497, **2023**.

[11] Wenzel, R. N. Surface roughness and contact angle. *The Journal of Physical Chemistry*, 53(9), 1466-1467, **1949**.